ROYAL SOCIETY
OF CHEMISTRY

PAPER

Mass-resolved UV–Vis–GPC mapping diagnoses catalyst ageing in RCF lignin streams

Siyuan Gao, [ID] Raul Rinken, Robert T. Woodward, [ID]† Jie Bao and Roberto Rinaldi [ID]*

Catalyst stability is central to the viability of lignin-first biorefineries, yet conventional characterisation often fails to detect the subtle deactivation processes that govern product quality. Here, we demonstrate that ultraviolet–visible (UV–Vis) spectroscopy, when combined with gel permeation chromatography (GPC), can serve as a sensitive diagnostic tool for detecting catalyst performance decline in Reductive Catalytic Fractionation (RCF). We introduce a concentration-independent spectral index (SI_{320}), derived from the absorbance ratio at 280 and 320 nm, given by $SI_{320} = 1 - A_{320}/A_{280}$. Native-like lignins show negligible absorbance at 320 nm ($SI_{320} \approx 1$), whereas condensation, benzylic oxidation, and extended π-conjugation depress SI_{320}. As a ratio, SI_{320} is concentration-independent within the Beer–Lambert regime and can be profiled across the chromatogram to yield $SI_{320}(M)$ profiles, with M denoting apparent molar mass. $SI_{320}(M)$ profiles report directly on the formation of chromophores associated with catalyst ageing across the lignin apparent-M distribution. Utilising post-consumer cardboard as a substrate, we tracked RCF over RANEY® Ni across multiple recycling runs. A comparative analysis of fresh and recycled catalysts revealed systematic SI_{320} downshifts in oligomer fractions, indicating chromophore accumulation well before changes in bulk yield of low M products become evident. Linear regression of $SI_{320}(M)$ mean values ($r^2 = 0.95$) enables a practical estimate of catalyst life. Under our conditions, it is estimated that RANEY® Ni can sustain lignin stabilisation for up to 15 runs of catalyst use (*ca.* 45 h operation), after which the chromophore density approaches that of organosolv lignin. Our findings reframe UV–Vis spectroscopy from a simple detection method for GPC analysis into a diagnostic platform of lignin-first catalysis. By funnelling apparent-M-resolved spectra into a simple index, GPC–UV–Vis enables rapid, non-destructive monitoring of catalyst performance, supports optimisation of RCF conditions and recycling protocols, and highlights the stabilising action of hydrogen-transfer catalysis. In the broader context,

Department of Chemical Engineering, Tomorrow's Chemical Technologies Lab, Imperial College London, South Kensington Campus, London, SW7 2AZ, UK. E-mail: r.rinaldi1@imperial.ac.uk

† Permanent address: Institute of Materials Chemistry and Research, Faculty of Chemistry, University of Vienna, Währinger Straße 42, Vienna, 1090, Austria.
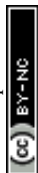
the approach is general to diverse feedstocks, catalysts, and lignin-first modalities, offering a practical route to correlate catalyst ageing with product quality and to guide development of durable, robust catalysts for circular economy and lignin valorisation.

Introduction

Lignin, a complex aromatic biopolymer in plant cell walls, is the most abundant renewable source of aromatic molecules and has attracted significant interest as a feedstock for sustainable biorefineries. However, its intrinsic structural heterogeneity (which varies with biomass source and even within a single lignin polymer) and its tendency to form recalcitrant linkages during extraction pose significant challenges to efficient valorisation.[1–5] In native biomass, lignin's three-dimensional network includes a variety of interunit bonds, primarily β-O-4 aryl–ether linkages along with C–C linkages.[2,5,6] Standard pulping or pretreatment processes often cleave the labile β-O-4 bonds, liberating reactive lignin fragments.[2,5,6] In the absence of stabilising reactions, these lignin fragments are prone to react, creating new non-native C–C interunit bonds. This condensation increases lignin's molar mass (M) and chemical complexity, yielding "repoly-merised" structures more resistant to depolymerisation, compared to native lignin structures.[2,5,7] Consequently, technical lignins isolated from harsh processes (*e.g.*, acid or alkaline pulping, Kraft pulping) typically have a substantially decreased β-O-4 content and a proliferation of carbon–carbon linkages in their polymeric structures, which significantly hinders their carbon- and energy-efficient upgrading *via* catalysis.[2] Such changes not only lower yields of low M products but also complicate the characterisation and reactivity of lignin.[8,9]

Renewed efforts in lignin research have underscored that how lignin is extracted and deconstructed is critical for its successful valorisation *via* catalysis.[2,5,10] This paradigm shift has given rise to so-called "lignin-first" biorefining strategies, which integrate biomass fractionation with immediate stabilisation of lignin fragments.[5] The goal is to preserve as much of lignin's native structure and functional groups as possible during extraction, thereby maximising its value. In practice, lignin-first approaches involve tandem extraction and *in situ* quenching of reactive intermediates – either through protective chemical agents[11] or catalytic transformations (reductive or oxidative)[5] – to prevent condensation.

In this context, Reductive Catalytic Fractionation (RCF) is a prominent lignin-first approach that employs a hydrogenation catalyst together with a hydrogen source (H_2 gas[12] or a hydrogen-donor solvent[7]) to solvolytically extract lignin from biomass and simultaneously stabilise it *via* selective hydrodeoxygenation (HDO) in addition to further depolymerisation of lignin fragments *via* hydrogenolysis of β-O-4 linkages. Altogether, these processes effectively quench the electrophilic sites and prevent the fragments from undergoing electrophilic aromatic substitution reactions (condensation).[5]

Under hydrogen-transfer RCF (HT-RCF) conditions using RANEY® Ni and 2-propanol as the H-donor, we recently demonstrated that the C_α–OH site in β-O-4 linkages is selectively reduced to a methylene group.[9] Introduction of this methylene group eliminates the possibility of forming a benzylic carbocation, thereby suppressing lignin condensation at that site.[9] These "reduced" β-O-4 structures appear as a signature of the hydrogenation catalyst's action even in

oligomeric and polymeric fractions. However, their relative abundance decreases with increasing M values.[9]

This observation reveals a new facet of the lignin-first paradigm: not only can RCF produce a stream of low-molar mass (LM) phenolic monomers, but it can also generate high-molar mass (HM) lignin fragments stabilised with controllable structural features. Therefore, through proper catalyst and condition choices, the lignin oligomers and polymers (in the 2–30 kDa range) can be recovered in a stabilised state, comprising both native and stabilised structures, rather than as highly condensed, intractable polymers.[9] Such stabilised oligomers and polymers could find use as functional macromolecules. Still, more importantly, their presence (and structure) can serve as an indicator of the efficacy of the lignin-first process in preserving lignin integrity *via* selective-HDO stabilisation.

Despite the clear benefits of lignin stabilisation during extraction, a practical challenge remains. How do we evaluate if and when a catalyst in an RCF begins to lose effectiveness? Metal catalysts may undergo gradual ageing or deactivation upon recycling (due to sintering, poisoning, fouling by deposits, to mention a few),[12] which could reduce their ability to cleave β-O-4 bonds or to perform selective HDO on the reactive sites that trigger condensation. A decline in this "stabilisation activity" might not be immediately evident from overall product yields (since lignin will still be extracted, albeit in a more degraded form). Thus, sensitive diagnostic methods are needed to detect subtle structural shifts in the lignin oil that would signal catalyst ageing – for example, an increase in the prevalence of condensation byproducts when the catalyst is reused.

Addressing this challenge requires analytical methods that can capture subtle changes in interunit linkages and functional groups, particularly those associated with condensation and other degradation pathways. NMR spectroscopy has long been the principal tool for detailed lignin analysis. Two-dimensional ^{1}H–^{13}C HSQC NMR is especially valuable, as it reveals characteristic bonding motifs (*e.g.* β-O-4 linkages, β-5 phenylcoumaran, β–β resinol, amongst other bonding motifs) alongside various pendant groups.[2,13] Advances in quantitative HSQC NMR methods have extended the utility of this technique.[8,14–16] In principle, HSQC NMR spectra from lignin oil obtained from successive RCF cycles could be compared to monitor the loss of specific linkages or the emergence of new features, such as condensed diarylmethanes, stilbenes, or oxidised benzylic carbons. In practice, however, the complexity of HSQC NMR spectra often obscures low-abundance structures.[17] Oligomeric and polymeric lignins generate broad, overlapping signals, and condensed units—present at only a few carbon sites—are easily masked by more intense resonances.[9,13,14,18]

Complementary information on functional groups can be obtained through derivatisation followed by ^{31}P or ^{19}F NMR spectroscopy. In these approaches, reactive sites such as hydroxyl groups are tagged *via* phosphitylating[19] or fluorinating[20] agents, enabling their selective detection and quantification. Such derivatisation circumvents some of the limitations of HSQC NMR analysis by providing a more quantitative profile of hydroxyl and related functionalities, although at the cost of additional sample preparation and chemical derivatisation.

While NMR-based approaches provide invaluable structural details, their inherent limitations—overlapping resonances, semi-quantitative cross-peak intensities, and substantial demands on sample purity and acquisition time—render them impractical for rapid diagnostics of catalyst performance. Herein, we repurpose ultraviolet–visible (UV–Vis) spectroscopy, coupled with gel permeation

Faraday Discussions

chromatography (GPC), as a complementary and more accessible tool to monitor catalyst ageing in reductive catalytic fractionation (RCF). A defining feature of lignin degradation is its progressive darkening,[21] driven by the accumulation of conjugated chromophores such as benzylic carbonyls, quinonoid moieties, and stilbene-type linkages, all of which extend absorption into the near-UV and visible regions.[22] We present a straightforward Spectral Index (SI) defined as $SI_{320} = 1 - A_{320}/A_{280}$, where A_{280} and A_{320} represent the absorbance measurements of eluting lignin species in GPC separation. This index measures the relative contribution of degradation-related chromophores while remaining unaffected by sample concentration within the Beer–Lambert law. Coupling SI with GPC allows continuous profiling across the chromatogram, yielding apparent-M-resolved profiles of chromophore occurrence. In practice, this enables direct tracking of the emergence of darkening species in specific fractions of the lignin stream—providing insight into how catalyst ageing influences lignin stabilisation and whether condensation products accumulate preferentially in HM fractions or are more broadly distributed.

The Results and discussion is organised into three sections. First, we benchmark HT-RCF against organosolv lignins, showing that reductive conditions limit chromophore formation, thereby suppressing long-wavelength absorbance ($\lambda \geq$ 320 nm). Second, we validate SI_{320} as a reliable diagnostic method by correlating SI_{320} trends with independent structural data from HSQC NMR spectroscopy and elemental analysis. Finally, we demonstrate the utility of SI_{320} in a recycling study utilising post-consumer cardboard, where M-resolved SI_{320} profiles exhibit a linear decline in hydrogenation capacity, which is otherwise insufficiently discernible through conventional bulk yield metrics. Taken together, these findings establish UV–Vis spectroscopy, long treated as a probe of lignin colour, as a quantitative and mechanistically meaningful diagnostic for lignin-first catalysis. The key lessons are that: (i) SI_{320} enables early and sensitive detection of catalyst deactivation; (ii) M-resolved SI_{320} profiles identify where in the lignin stream degradation accumulates, providing mechanistic insight; and (iii) the method is rapid, non-destructive, and transferable, making it ideally suited for online monitoring and process optimisation in lignin valorisation.

Experimental

Chemicals

Poplar wood chips (2 mm) were purchased from J. Rettenmaier & Söhne. Post-consumer cardboard was sourced from Amazon UK. Tetrahydrofuran (inhibitor-free for HPLC, ≥99.9%), dimethyl sulfoxide-d₆ (99.9 atom% D), methanol (≥99.9%, analytical grade), lithium bromide (≥99.9%, Aldrich), and RANEY® Ni 2800 slurry were obtained from Sigma-Aldrich and used as received. 2-Propanol (≥99.9%) was purchased from Fluka. *N,N*-Dimethylformamide (DMF, >99.5%, HPLC grade) was purchased from VWR and used without further purification. GPC polystyrene (PS) standard ReadyCal set ($M_p \sim$ 250–65000 Da) was obtained from Supelco.

Organosolv extraction

Poplar wood chips (16–17 g) or post-consumer cardboard (10 g) were suspended in a 2-propanol/water solution (140 mL, 7 : 3 v/v) in a 250 mL autoclave equipped with
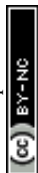
a mechanical stirrer. The mixture was heated to 200 °C over 1 h under continuous stirring and maintained at this temperature under autogenous pressure for 3 h. After cooling to room temperature, the reddish-brown liquor was separated from the solid residue (pulp) by filtration through a glass fibre filter (GF6, Ø 90 mm, Whatman). The liquor was concentrated by partially evaporating 2-propanol at 60 °C using a Hei-dolph rotary evaporator, inducing lignin precipitation. The precipitated solid was collected by filtration, resuspended in hot water to remove residual hemicellulose sugars, and filtered again. The resulting solid was washed several times with hot water and dried in a vacuum oven at 40 °C overnight to yield organosolv lignin.

HT-RCF experiments

Poplar wood (16–17 g) or post-consumer cardboard (10 g, dry weight, blended) was added to a suspension of RANEY® Ni (10 g, wet basis) in a 2-propanol/water solution (140 mL for poplar wood or 170 mL for cardboard, 7 : 3 v/v) in a 250 mL autoclave equipped with a mechanical stirrer. The suspension was heated to 200 °C over 1 h under continuous stirring. The HT-RCF processing time was recorded from this point, and the reaction was maintained at this temperature under autogenous pressure for 3 h (or for different durations in the time-resolved experiments on monomer yield evolution during HT-RCF of post-consumer cardboard). After cooling to room temperature, the liquor was separated from the solids (RANEY® Ni and pulp) by filtration through a glass fibre filter (GF6, Ø 90 mm, Whatman). The wet solids were transferred to a 250 mL round-bottom flask containing 2-propanol and resuspended under overhead stirring. RANEY® Ni was separated magnetically by placing a magnet externally at the bottom of the flask. This resuspension and magnetic separation procedure was repeated 5–6 times until the catalyst was entirely removed from the pulp fibres. The pulp fibres, which remained suspended, were recovered by filtration. The spent catalyst was washed and stored in 2-propanol for recycling experiments. The liquor and all filtrates from the catalyst separation procedure were combined, and the lignin oil was recovered by removing the solvent at 60 °C under reduced pressure using a rotary evaporator (poplar lignin oil) or a centrifugal evaporator (cardboard lignin oil). The poplar lignin oil was collected and stored in a vacuum oven at 40 °C overnight. In comparison, the cardboard lignin oil was further treated in a rotary evaporator at 45 °C for 4 h under reduced pressure (80 mbar). Solvent removal was carried out gently to minimise the loss of alkyl cyclohexanol products (present in the cardboard lignin oil).

Gas chromatography analysis

An aliquot of each sample (50.0 mg) was suspended in ethyl acetate (2 mL) containing the internal standard n-decane at 1 mg mL^{-1}. The suspension was centrifuged, the supernatant collected, and then filtered through a 0.45 μm membrane filter. Next, the clear yellowish sample solutions were analysed using a gas chromatograph (GC-2010 Plus, Shimadzu) equipped with a flame ionisation detector (FID) and a mass spectrometer detector (MSD), fitted with a DB-1MS capillary column (30 m × 0.25 mm i.d., film thickness 0.25 μm). The oven temperature programme was as follows: initial isothermal step at 40 °C for 5 min, followed by a ramp at 5.2 °C min^{-1} to 320 °C, held for 5 min. Products were identified by matching the mass spectra to the NIST 08, NIST 08s, and Wiley 9 MS libraries. Quantification of identified products was performed using the FID

response for authentic product standards, or, when standards were not available, by applying their effective carbon numbers.

Pulp compositional analysis

The contents of glucan, xylan, and lignin were determined by the sulphuric acid saccharification method following the general guidelines by the National Renewable Energy Laboratory (NREL).[23] In a typical procedure, 0.30000 g of sample was suspended in 3 mL of 72% sulphuric acid and maintained at 33 °C for 1 h. Subsequently, 84 mL of deionised water was added, diluting the acid concentration to 4%. The mixture was then heated in an autoclave at 121 °C for 1 h. After cooling to room temperature, the suspension and liquor were separated by filtration through a 0.45 μm nylon filter. The solid residue, dried in a vacuum oven for 48 h, was taken as the acid-insoluble lignin (Klason lignin). The filtrate, containing dissolved glucose and xylose, was analysed by using an HPLC (PerkinElmer Series 200) equipped with a Nucleogel Ion 300 OA column (Macherey-Nagel). HPLC analysis was conducted at 80 °C using 5 mmol L^{-1} H_2SO_4 as the mobile phase (0.60 mL min^{-1}).

The acid-soluble lignin content was determined from a 1 : 7 (v/v) diluted aliquot of the filtrate using a UV–Vis spectrometer (Agilent 8453 UV-visible spectroscopy system). All calculations were normalised to the initial sample mass to account for water loss during the autoclaving step.

The moisture content of cardboard and pulp samples was measured using a Mettler Toledo HE73 moisture analyser. For each measurement, 0.5–1.0 g of sample was heated to 105 °C, and the weight loss was recorded.

Ash content was determined following the NREL method.[24] Approximately 0.5 g of sample was placed in a ceramic crucible and incinerated in a ventilated muffle furnace at 575 °C for 4 h. The crucibles were cooled to room temperature in a desiccator before weighing.

Key performance indicators for HT-RCF and organosolv processing of post-consumer cardboard (glucan retention, xylan retention, and delignification) were calculated according to eqn (1) to (3):

$$\text{Glucan retention}(\%) = \frac{m_{\text{pulp,out}} \times w_{\text{glucan,pulp}}}{m_{\text{cardboard,in}} \times w_{\text{glucan,cardboard}}} \times 100 \tag{1}$$

$$\text{Xylan retention}(\%) = \frac{m_{\text{pulp,out}} \times w_{\text{xylan,pulp}}}{m_{\text{cardboard,in}} \times w_{\text{xylan,cardboard}}} \times 100 \tag{2}$$

$$\text{Delignification}(\%) = \left(1 - \frac{m_{\text{pulp,out}} \times w_{\text{lignin,pulp}}}{m_{\text{cardboard,in}} \times w_{\text{lignin,cardboard}}}\right) \times 100 \tag{3}$$

where: $m_{\text{cardboard,in}}$ and $m_{\text{pulp,out}}$ correspond to the masses of input cardboard before processing and recovered pulp after processing, respectively; $w_{\text{component,cardboard}}$ and $w_{\text{component,pulp}}$ denote the mass fraction of the component of interest (i.e., glucan, xylan, lignin) in the input cardboard and the recovered pulp, respectively. All masses are dry-based and expressed in grams (g).

Preparative GPC

Tetrahydrofuran/deionised water (90 : 10 v/v) was used as the mobile phase. A sample of poplar wood lignin (1 g, HT-RCF lignin oil or organosolv lignin) was
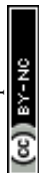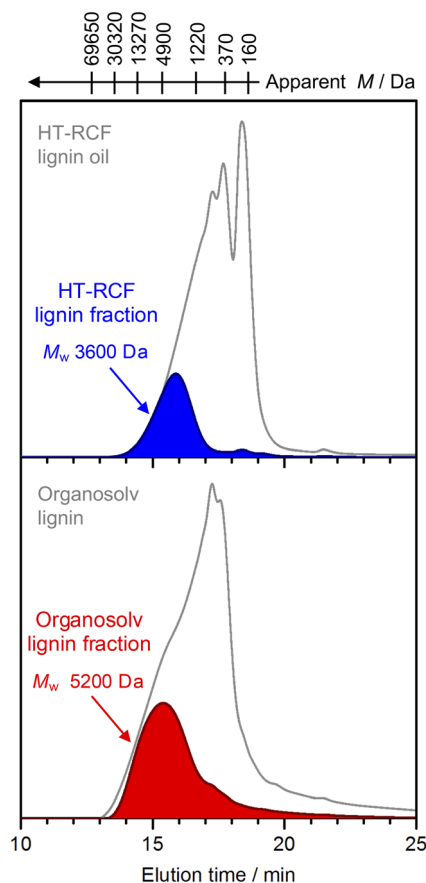
Fig. 1 Analytical GPC chromatograms of lignin streams from HT–RCF (top) and organosolv (bottom) processing of poplar (200 °C, 3 h). Grey traces: whole lignin streams. Coloured fills: HM-fractions isolated by preparative GPC (HT–RCF lignin oil: $M_w = 3600$ Da, organosolv lignin: $M_w = 5200$ Da). The upper axis reports apparent molar mass (Da); earlier elution corresponds to higher apparent molar mass.

dissolved in 8–10 mL of the eluent and filtered before injection (0.45 μm nylon filter). Aliquots of 200–1000 μL were injected into a Shimadzu liquid chromatograph equipped with a preparative GPC column (Agilent PLgel 10 μm MIXED-D, 25 mm × 300 mm) operating at a flow rate of 3 mL min⁻¹. Detection was performed using a UV–Vis detector (SPD-20A, Shimadzu) with a short-path cell, set at 254 nm. Samples were fractionated into at least five fractions based on molecular weight. For this study, the analysis focused on the heaviest fraction obtained, as shown in Fig. 1.

Analytical GPC

To analyse the apparent molar mass distributions, all samples (5–20 mg) were dissolved in DMF (1 mL) containing LiBr (0.1 wt%) and were filtered before injection (0.45 μm nylon filter). The injection volume was 10 μL. For the apparent M data, GPC analyses were performed employing a set of three columns (guard
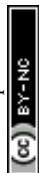
column: 1 × PolarGel-M, separation columns: 1 × PolarGel-M and 1 × PolarGel-L, 7.8-mm diameter and 300-mm length, Agilent Technologies) operating at 60 °C. The eluent flow rate was 1 mL min^{-1}. The analysis was carried out on an HPLC (Prominence system, Shimadzu) equipped with a refractive index detector (operating at 40 °C, RID-20A, Shimadzu) and a photodiode array detector (PDA, operating at 25 °C, SPD-M20A, Shimadzu). Data treatment was performed using Shimadzu GPC software suite (Shimadzu LabSolutions, version 5.98). The apparent M values are given relative to polystyrene M calibration.

Determination of the spectral index (SI$_{320}$)

The values for SI$_{320}$ were calculated according to eqn (4), *vide infra*. Background subtraction was performed using the eluent chromatogram as the baseline, applying the Shimadzu LabSolutions software with the GPC add-on suite (version 5.98). The background-subtracted chromatogram data, recorded at the required wavelengths (bandwidth ±4 nm), were subsequently exported to OriginLab 2025 for SI$_{320}$ calculation and plotting. For consistency and to minimise artefacts arising from the low concentration of eluting lignin species, the lower and upper M cut-off values for SI calculation were defined as the points corresponding to approximately 5% of the maximum detector response at 280 nm, unless stated otherwise. The mean SI value for each sample was calculated from all SI data points within this range, and the standard deviation (s.d.) was determined accordingly.

HSQC NMR spectra measurements

HT-RCF or organosolv poplar wood lignin fraction (20 mg) was dissolved in DMSO-d_6 (1 mL) and transferred to an NMR tube for analysis. All spectra were obtained at 25 °C using a Bruker AV spectrometer (500 MHz ^{1}H-frequency) equipped with a BBFO probe head with z-gradient. The 2D HSQC NMR (Bruker standard pulse sequence "*hsqcetgpsi*" with delay optimised for $^1J_{CH}$ of 145 Hz) was set up with spectral widths of 20 ppm and 180 ppm for ^{1}H and ^{13}C dimensions, respectively. The number of collected complex points was 2048 for ^{1}H-dimension with a recycle delay of 3.13 s (3.0 s relaxation delay and 0.13 s acquisition time). The number of transients for the HSQC NMR spectra was between 12 and 24, and 512-time increments were recorded in the ^{13}C dimension, resulting in an overall experimental time of 6–12 h. For HSQC NMR experiments, a squared cosine-bell apodization function was applied in both dimensions, followed by zero-filling to 1024 points in the ^{13}C dimension before Fourier transform. All spectra were processed using MestReNova software (14.3.3). Cautious interpretation of HSQC NMR spectrum data is required, as in regular HSQC pulse sequences, the $^1J_{CH}$ dependence of polarisation transfer is not suppressed. Consequently, the absolute intensity of cross-signals is not fully universal in the entire spectral range. Valuable semi-quantitative information can still be obtained through regular HSQC NMR measurements for characterisation and comparison of lignins. Semi-quantitative determination of volume integral ratios is possible for ^{1}H–^{13}C pairs in a similar chemical environment, as the $^1J_{CH}$ values for specific entities are reasonably comparable. Semi-quantitative analysis was performed separately for different regions of the HSQC NMR spectra by integration of ^{1}H–^{13}C pairs of interest, as presented in ref. 9.

Elemental analysis

CHN/O analysis of materials was performed on an Elementar VarioMICRO Cube. Samples (*ca.* 2 mg) were weighed and sealed in a tin boat prior to analysis. Each sample was measured at least in triplicate. Oxygen content was determined by subtraction (%O = 100 − %C − %H − %N − %ash).

Results and discussion

### Comparison of RCF lignin and organosolv lignin

To benchmark the effect of reductive catalytic processes on lignin structure, we compared lignin streams derived from HT-RCF and an organosolv process applied to poplar wood, each conducted in 2-propanol/water (70 : 30, v/v) at 200 °C for 3 h. HT-RCF was performed in the presence of RANEY® Ni, while the organosolv process was carried out with no added catalyst. In this comparative analysis, we focused on HM-lignin fractions with overlapping distributions and isolated them from each stream by preparative GPC. As shown in Fig. 1, preparative GPC furnished HM fractions with comparable apparent M distributions. The weight-average molecular weights (M_w) of these fractions are 3600 Da for the HT-RCF lignin fraction and 5200 Da for the organosolv lignin fraction.

To assess the structural differences between the fractions, we examined the 2D HSQC NMR spectra of the HT-RCF and organosolv lignins (Fig. 2). Summarised in Table 1 is the estimated distribution of lignin linkages per 100 aromatic units.

In the aliphatic oxygenated region, the most distinguishing feature of the HT-RCF lignin spectrum is an additional triad of cross-signals absent from the organosolv counterpart (Fig. 2a). This triad is unambiguously assigned to reduced β-O-4 motif linking two syringyl units, $A_{(CH_2)}$–SS.[9] The benzylic methylene at C_α gives two ^{13}C–^1H cross-peaks at δ_C/δ_H 36.88/2.86 and 36.88/2.77 ppm, consistent with diastereotopic α-protons on the same carbon. The β position appears as a single correlation at 82.91/4.14 ppm, while the γ-CH_2 correlations—despite lying in a congested part of the spectrum—can be discerned at 61.30/3.41 ppm. All chemical shifts are in excellent agreement with literature values for $A_{(CH_2)}$–SS in lignin model compounds and isolated lignans.[25–28]

HT-RCF lignin contains 2.9 ± 0.2 reduced β-O-4 linkages [$A_{(CH_2)}$] per 100 Ar units, *versus* none in organosolv lignin. Relative to organosolv, the HT-RCF fraction is depleted in phenylcoumaran (β-5, B) and resinol (β–β, C) substructures (B: 2.1 ± 0.1 *vs.* 6.8 ± 0.4; C: 5.2 ± 0.4 *vs.* 7.9 ± 0.5 per 100 Ar units). The β-5 depletion exceeds what would be expected solely from the decrease in G-units in RCF lignin, but is consistent with (i) α-O-4 hydrogenolysis within phenylcoumaran bonding motifs (B) and (ii) the lower guaiacyl (G) content of the HT-RCF fraction (*vide infra*).

HT-RCF lignin fraction is enriched in syringyl units, with an estimated content of S-units of 72.3 ± 0.4% *versus* 64.8 ± 0.8% for organosolv. This is consistent with two effects: (i) selectivity, whereby RANEY®-Ni/2-propanol preferentially transforms the less sterically hindered, G-rich lignin fragments;[29] and (ii) fractionation kinetics, as G-rich lignin fragments are released early in RCF (<1 h) and, in batch operation, dwell longer in the liquor, increasing their probability of further conversion to low-M products.[30,31] In line with this, our previous report showed that the 200–1000 Da fraction is G-enriched relative to mid- and HM fractions.[9] As
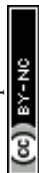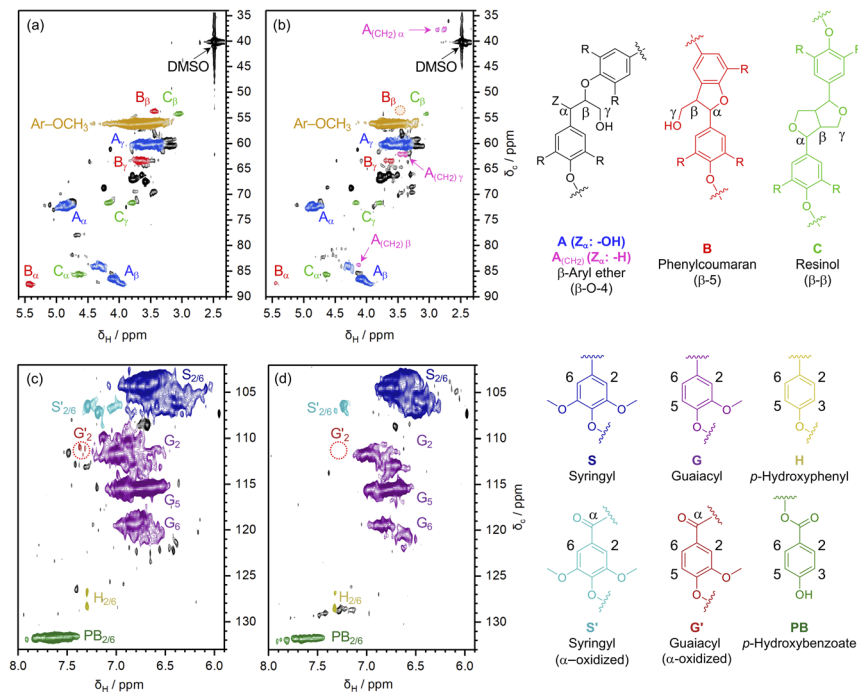
Fig. 2 HSQC NMR spectra (DMSO-d_6) of high-MW fractions: (a) organosolv lignin, oxygenated aliphatic region; (b) HT-RCF lignin, oxygenated aliphatic region; (c) organosolv lignin, aromatic region; (d) HT-RCF lignin, aromatic region. Coloured overlays highlight regions pinpointing β-O-4 (A, including reduced β-O-4 with $C_\alpha H_2$, A_{CH_2}, β-5 (phenyl-coumaran, B) and β–β (resinol, C) substructures. Note: in (d), the B_β cross-signal lies below the displayed intensity threshold but is detectable upon zooming in. Stilbene bonding motifs were not visible in the HSQC NMR spectra.

expected, oxidised S′ and G′ units are also suppressed under HT-RCF. Oxidised S′ units decrease from $5.5 \pm 0.9\%$ (organosolv) to $2.3 \pm 0.1\%$ (HT-RCF), while oxidised G′ units drop from $0.9 \pm 0.1\%$ to below detection.

Elemental analysis corroborates the reductive transformations in the HT-RCF fraction. The O/C ratios of the high-MW fractions are similar (HT-RCF 0.39 ± 0.05

Table 1 Estimated distribution of lignin linkages per 100 aromatic units

Linkage or unit	HT-RCF lignin fraction	Organosolv lignin fraction
A (β-O-4)	39.8 ± 1.2	40.1 ± 0.5
$A_{(CH_2)}$ (reduced β-O-4)	2.9 ± 0.2	0.00
A (total)	42.6 ± 1.2	40.1 ± 0.5
B (β-5)	2.1 ± 0.1	6.8 ± 0.4
C (β–β)	5.2 ± 0.4	7.9 ± 0.5
$[(S_{total})/(S_{total} + G_{total})] \times 100^a$	$72.3 \pm 0.4\%$	$64.8 \pm 0.8\%$
$[S'/(S_{total} + G_{total})] \times 100^a$	$2.3 \pm 0.1\%$	$5.5 \pm 0.9\%$

^{a} $S_{total} = S + S'$; $G_{total} = G + G'$.
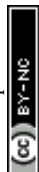
and organosolv 0.42 ± 0.06) and close to the value expected for hardwood lignin (≈ 0.44),[9] indicating a comparable overall O/C ratio. By contrast, the HT-RCF fraction shows a higher H/C ratio (1.31 ± 0.05) than both organosolv (1.16 ± 0.04) and the nominal hardwood benchmark (≈ 1.25). Relative to the organosolv lignin fraction, this $\Delta(H/C) = 0.15$ corresponds to $\approx 1.5 \pm 0.5$ additional H atoms per C_9 phenyl-propane unit, consistent with benzylic/sidechain HDO under HT-RCF conditions.

UV–Vis-resolved GPC distinguishes HT-RCF and organosolv lignins

The UV–Vis spectrum of lignin, particularly in the long-wavelength region (>320 nm, UV-A and visible), is highly sensitive to alterations in chemical structure. Structural modifications that extend π-conjugation—through oxidation, condensation, or unsaturated linkages—generate additional chromophores and increase visible-light absorption, imparting a darker colour.[21,32,33] Conversely, processes that break conjugation or remove such moieties reduce UVA and visible absorbance, effectively "bleaching" the lignin.

To investigate chemical differences beyond apparent-M distribution, we examined the apparent-M-resolved UV–Vis spectra of the species eluting during GPC (Fig. 3). This approach resolves the distribution of chromophores across the apparent-M range and reveals structural distinctions between HT-RCF and organosolv lignins not evident from size data alone.

In the GPC-eluting species of the HT-RCF lignin fraction in 0.1 wt% LiBr/DMF (Fig. 3a), the online UV–Vis profile is spectrally uniform across the elution window and dominated by a band at ~280–285 nm, assigned to the ^1L_b band in substituted benzenes.[34] In addition, offline UV–Vis measurement of the whole HT-RCF lignin fraction in $CH_3OH–H_2O$ (7 : 3, v/v) (Fig. 3c) provides access to the short-wavelength region, where the steep rise at 200–210 nm corresponds to the ^1L_a band in substituted benzenes.[34] A subtle shoulder at 230–255 nm originates from the higher-energy $\pi \rightarrow \pi^*$ vibronic structure of anisole-type rings, which is red-shifted and broadened by methoxy substitution. Notably, absorbance falls sharply above 280 nm. The absence of significant features in this region indicates that transitions associated with degradation-derived chromophores—$n \rightarrow \pi^*$ excitations of aryl carbonyls (benzylic ketones, aldehydes, Hibbert-ketone-type species), $\pi \rightarrow \pi^*$ transitions of α,β-unsaturated carbonyls weakly conjugated to the ring, $\pi \rightarrow \pi^*$ bands of quinonoid structures, and intramolecular charge-transfer (CT) between phenolate donors and quinone/carbonyl acceptors—are negligible. Under HT-RCF conditions, such chromophores are selectively hydrogenated or otherwise saturated, preserving native-like aromatic substitution patterns and preventing the formation of new UV-A/visible-absorbing structures.[22]

The organosolv lignin fraction (Fig. 3b) shows a markedly different profile, with a broadened absorption envelope extending from the ~280 nm aromatic maximum into the visible region (up to ~550 nm). As presented in Fig. 3c, the pronounced shoulder at ~300–320 nm arises from a combination of $n \rightarrow \pi^*$ transitions of aryl carbonyls (α-carbonyl phenolics, benzylic ketones/aldehydes) and $\pi \rightarrow \pi^*$ transitions of α,β-unsaturated carbonyls partially conjugated with the aromatic ring. The broader band at ~330–370 nm is characteristic of $\pi \rightarrow \pi^*$ transitions of quinonoid structures (p-quinones, o-quinones) and CT transitions involving phenolate donors and quinone/carbonyl acceptors,[22,34] both of which are typically generated during acidic, thermal organosolv processing via
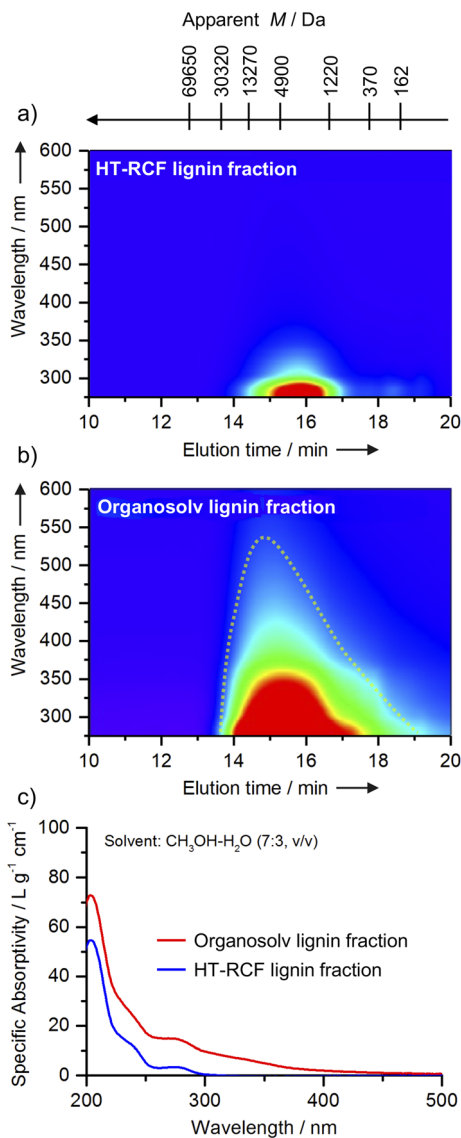
Fig. 3 UV–Vis-resolved GPC analyses provide a comparative assessment of the HM fractions derived from HT-RCF lignin and organosolv lignin. All GPC measurements were performed using 0.1 wt% LiBr/DMF as the eluent. In panel (a), the HT-RCF fraction exhibits pronounced absorption within the ultraviolet region (280–300 nm), while absorbance above 320 nm remains minimal. In contrast, panel (b) reveals that the organosolv fraction displays a broader absorption spectrum, extending from 280 nm well into the visible region (up to 550 nm). Panel (c) presents overlaid UV–Vis spectra for these fractions, measured in $CH_3OH–H_2O$ (7 : 3, v/v). This comparison clearly illustrates a strong long-wavelength absorption tail for organosolv lignin (red curve) compared to the HT-RCF lignin (blue curve). Such spectral differences are indicative of an increased population of conjugated chromophores within the organosolv sample. These findings highlight the substantial impact of HT-RCF processing on the decrease in chromophore content and the distinguished electronic structure of the resulting lignin fractions.

condensation, hydrolysis, and oxidation. The smooth tail from ∼380 nm to 500 nm is attributed to low-oscillator-strength CT bands and $\pi \rightarrow \pi^*$ transitions of extended π-systems such as stilbene-type diarylalkenes and highly conjugated enones, often embedded within condensed aromatic domains.[22,34] None of these long-wavelength features are present in native lignin;[35] they are clear signatures of chemical alteration during organosolv pulping.

The overlaid spectra in Fig. 3c, recorded in CH_3OH/H_2O (7 : 3, v/v), highlight these distinctions: organosolv lignin exhibits substantial absorption above 280 nm, whereas HT-RCF lignin shows an abrupt decline. These results reflect the chemical selectivity of reductive catalytic fractionation, which not only solubilises lignin but also stabilises it through hydrogenolysis of aryl–ether bonds and hydrogenation/HDO of unsaturated and carbonyl functionalities. In the presence of RANEY® Ni and 2-propanol as hydrogen donor, reactive α,β-unsaturated linkages and benzylic carbonyls are rapidly reduced to saturated methylene or methyl groups.[9,29,32,36–38] This both inhibits condensation and removes existing chromophores—functional groups that also serve as reactive sites for re-polymerisation.

Spectral index (SI) as a metric for assessing hydrogenation catalyst activity

In addition to providing molar-mass distribution, GPC serves as an analytical fractionation tool that enables M-resolved spectroscopic profiling of lignin heterogeneity in a single experiment. This approach is still underutilised in lignin characterisation. Coupling GPC with online UV–Vis detection provides a rapid and low-overhead method for profiling structural changes across the elution window, eliminating the need for additional sample handling.

For a quantitative assessment of the degradation-derived chromophores, we propose the Spectral Index (SI_λ) using a chosen long-wavelength probe ($\lambda \geq 320$ nm), which in this study is set at 320 nm, as per eqn (4):

$$SI_{320} = 1 - \frac{A_{320}}{A_{280}} \qquad (4)$$

where A_{280} is the absorbance at 280 nm ($\pi \rightarrow \pi^*$ ^1L_b transition of G/S aromatic units), and A_{320} is the absorbance at 320 nm, where native-like lignins start to exhibit negligible intensity.[39] Such native-like lignins—including β-O-4, β-5, and β–β model compounds, milled-wood lignin, and dehydrogenation polymers (DHPs)—give $SI_\lambda \approx 1$ for long-wavelength $\lambda \geq 320$ nm. We extrapolate that RCF would go further and, by eliminating existing chromophores, it also leads to SI_λ values tending towards 1. Conversely, upon catalyst ageing or deactivation, degradation-derived chromophores accumulate through condensation, benzylic oxidation, or extension of π-conjugation. In this manner, A_λ increases, and SI_λ value decreases.

Because SI_{320} is defined as a ratio of absorbances at two wavelengths, it is independent of analyte concentration and optical path length within the linear range of the Beer–Lambert law. This makes it well suited for M-resolved analysis. SI_λ can thus be calculated continuously across the chromatogram to produce $SI_{320}(M)$ profiles. Averaging SI values over defined apparent M windows provides an estimate of the prevalence of long-wavelength chromophores in those fractions. In contrast, the standard deviation within each window offers a quantitative measure of structural heterogeneity.
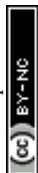
Fig. 4 presents the $SI_{320}(M)$ profiles for the lignin fractions. The HT-RCF lignin fraction exhibits a broader distribution of SI_{320} values, with a mean of 0.83 ± 0.03, in contrast to the organosolv fraction, which displays a narrower spread and a lower mean of 0.550 ± 0.003. While HSQC NMR provides valuable semi-quantitative information on specific motifs—most notably the formation of reduced β-O-4 linkages and the decrease in S′ and G′ units oxidised at the C_α position (Fig. 2 and Table 1)—its ability becomes limited when probing minor chromophoric features dispersed across the lignin stream. By comparison, the SI_{320} metric reveals these subtle, distributed structural changes with much greater sensitivity, offering a more comprehensive fingerprint of catalyst performance and lignin stabilisation. Thus, the SI_{320} metric should be regarded as complementary to HSQC NMR. Whereas HSQC NMR can semi-quantitatively track specific motifs, $SI_{320}(M)$ profile provides a broader and more sensitive readout of chromophoric changes occurring across the apparent M range of the lignin stream.

In a previous work, we demonstrated that lignin fragments containing reduced β-O-4 linkages—formed via selective HDO at the C_α position of native β-O-4 motifs—are present throughout the lignin fragment population.[9] However, the fraction of reduced β-O-4 units decreases exponentially from ca. 21% at M_w 500 Da to only 0.7% at M_w 16 900 Da.[9] This trend arises because large lignin fragments experience significant steric hindrance, limiting access to the catalyst surface and thereby reducing the probability of undergoing the C_α-HDO reaction. In Fig. 4, the $SI_{320}(M)$ profile for the RCF lignin fraction mirrors this behaviour. Low-M eluting lignin species, where reductive catalytic processes are most effective, exhibit the highest SI_{320} values (minimal long-wavelength absorbance). In contrast, high-M eluting lignin species show a modest decline in SI_{320} as some residual
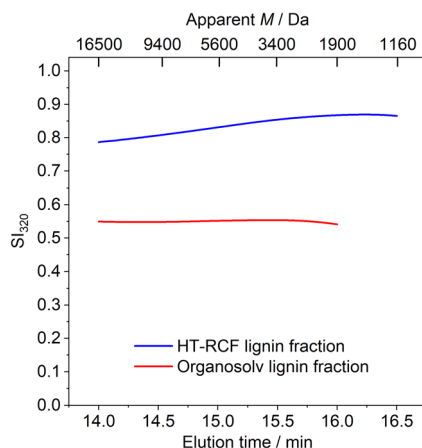

Fig. 4 $SI_{320}(M)$ profiles for the HM fractions of HT–RCF lignin (blue) and organosolv lignin (red), derived from GPC–UV analysis. The HT-RCF fraction shows a higher mean SI_{320} value (0.83 ± 0.03) and greater variation across the apparent M range, reflecting the heterogeneous suppression of chromophores by selective HDO of β-O-4 linkages. The $SI_{320}(M)$ profile declines gradually with increasing apparent M values due to steric hindrance, which limits catalyst access to larger lignin fragments. In contrast, the organosolv lignin fraction exhibits a lower mean SI_{320} value (0.550 ± 0.003) and a narrow distribution, consistent with uniform and extensive degradation of native lignin structures in the absence of a stabilisation step.
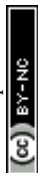
chromophores persist. Nevertheless, even in the highest-M region, the HT-RCF lignin maintains a substantially higher SI_{320} than the organosolv fraction, underscoring the persistent benefit of reductive processes on lignin stabilisation.

In contrast, the organosolv lignin fraction exhibits a remarkably narrow SI_{320} range (standard deviation only 0.0026). This uniformity reflects the absence of a stabilisation mechanism. It reveals that the degradation of native lignin structures occurs uniformly in terms of chromophore formation across the M range. The resulting chromophore population, generated through condensation, oxidation, and solvolysis, is consistently distributed, resulting in a low and flat $SI_{320}(M)$ profile.

Case study: catalyst ageing in HT-RCF of cardboard

Cardboard constitutes a significant fraction of lignocellulosic packaging materials in the UK, with a consumption of 5.4 Mt recorded in 2021.[40] While approximately 70% of UK paper and cardboard packaging is mechanically recycled,[40] repeated re-pulping progressively shortens fibre length and compromises mechanical integrity, ultimately rendering the fibres unsuitable for packaging applications.[41] Developing valorisation pathways capable of recovering both the fibre and lignin fractions from end-of-life cardboard could extend the material's functional lifespan, alleviate pressure on virgin forest resources, and align with circular-economy principles by maintaining materials in productive use for longer.

The post-consumer cardboard employed in this study comprised 57% cellulose, 18% Klason lignin, 13% hemicellulose, and 12% ash. The relatively high lignin content positions this residue as a promising feedstock for RCF. However, because cardboard production involves prior chemical and/or mechanical pulping, the lignin present is no longer native. Still, it consists of residual lignin with structural modifications, including condensation and partial oxidation, arising from previous processing steps. These structural alterations are expected to influence both reactivity and product distribution in the HT-RCF process.

In this section, we present preliminary results on HT-RCF of post-consumer cardboard as a case study to evaluate the SI_{320} as a metric for assessing catalyst ageing during recycling. HT-RCF of post-consumer cardboard was conducted with RANEY® Ni in 2-propanol/H_2O (7 : 3, v/v) at 200 °C for 3 h. After each run, the catalyst was magnetically recovered, washed, and reused for four further cycles. Across runs 1–5, we monitored three core pulp-quality key performance indicators (KPIs)—delignification, glucan retention, and xylan retention—and benchmarked the pulps against an organosolv reference. Fig. 5 summarises the evolution of KPI values over the catalyst recycling test.

Fig. 5 shows that delignification under HT-RCF remains broadly stable ($\approx$47–54%) across the recycle series, with only modest variability; the organosolv reference is slightly lower ($\approx$42–43%). The enhanced delignification under HT-RCF is attributed to the stabilisation of solubilised lignin fragments in the liquor, which prevents these fragments from condensing onto the fibre surface, thereby facilitating more complete lignin removal. Moreover, glucan retention is consistently high for HT-RCF ($\approx$90–92%) and exceeds the organosolv value ($\approx$82–84%), indicating that cellulose integrity is well preserved throughout the catalyst recycling tests.
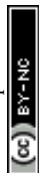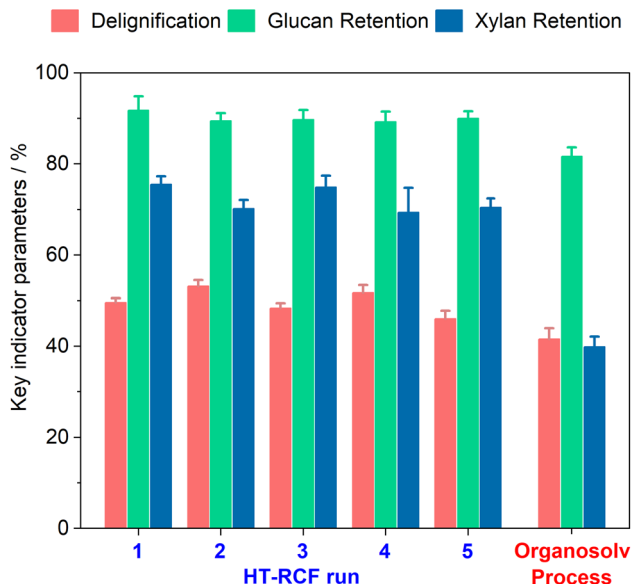
Fig. 5 Pulp-quality metrics during catalyst recycling in HT-RCF of post-consumer card-board, benchmarked against an organosolv control. Bars indicate delignification, glucan retention, and xylan retention; values are mean ± s.d. for the fresh catalyst and each recycle. The rightmost group corresponds to the organosolv reference at matched severity (no catalyst). HT-RCF conditions: 10 g cardboard (dry basis), 10 g RANEY® Ni (wet basis), 200 °C, 170 mL 2-propanol/water (7 : 3 v/v), 3 h.

The most discriminating KPI is xylan retention. HT-RCF maintains ≈70–77% across all runs, whereas the organosolv process retains only ≈40–42%. Even after five cycles of RANEY® Ni use, HT-RCF outperforms organosolv in conserving hemicellulose content in the pulp, making xylan retention a sensitive and reliable metric for differentiating the two processes in terms of pulp quality.

The superior performance of HT-RCF in preserving xylans and glucans in the pulps is consistent with our previous mechanistic study of liquors produced in 2-propanol/water at 200 °C.[42] In that work, we demonstrated that, in the presence of RANEY® Ni, C_5/C_6 sugars released during cooking are rapidly hydrogenated to the corresponding sugar alcohols (*e.g.*, xylitol, sorbitol).[42] This hydrogenation step suppresses dehydration to furfurals and the subsequent formation of formic acid, thereby limiting acid build-up and the acid-catalysed hydrolysis of hemicelluloses and, to a lesser extent, cellulose. In contrast, organosolv liquors accumulate substantially more formic acid.[42] This factor promotes hemicellulose loss and lower xylan retention under HT-RCF conditions.[42,43]

Before the recycling tests, we examined the kinetic profile of HT-RCF of post-consumer cardboard to track the evolution of lignin-derived monomers under hydrogen-transfer conditions (Scheme 1b). At 200 °C, depolymerisation begins during the heat-up process, with trace monomers already detected at the "0 h" mark. The total yield of aromatic phenols rises rapidly within the first hour, consistent with solvolysis and initial hydrogenolysis of the lignin matrix. With longer reaction times, these phenols are partially converted into alkyl phenols,

indicating sidechain cracking *via* hydrogenolysis or dehydration–hydrogenation of the terminal –CH_2OH group. After 2 h, phenolic yields decline sharply, while cyclohexanol-type products increase, marking a shift from monomer release to aromatic-ring saturation. The first dominant saturated product is 4-(3-hydroxypropyl)cyclohexanol, which retains the terminal alcohol group, whereas by 3–4 h the main product becomes 4-ethylcyclohexanol.

The kinetic monitoring trends support a two-stage view of HT-RCF of cardboard (Scheme 1a): (i) an early lignin-first depolymerisation and hydrogenolysis phase that liberates phenolic monomers, followed by (ii) a deep-upgrading phase in which those monomers undergo rapid ring hydrogenation and, to a lesser extent, C–C/C–O scission on the side chain, as reported in flow systems.[30,46–49] The unusual extent of aromatic-ring saturation at 200 °C—without external H_2—
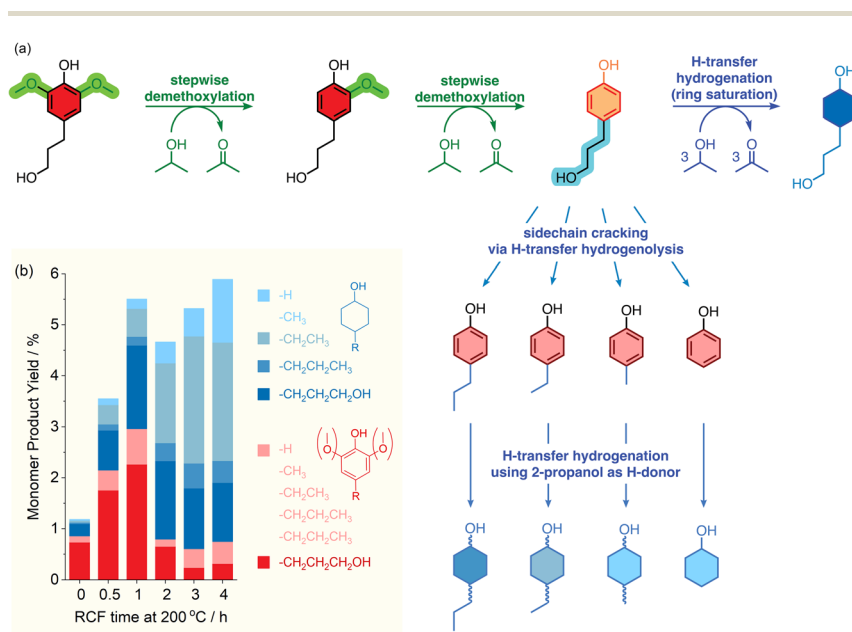
Scheme 1 (a) Proposed reaction network for HT-RCF over RANEY® Ni using 2-propanol as the H-donor. Lignin fragments undergo selective HDO, forming dihydrolignols, which then undergo stepwise demethoxylation (syringyl → guaiacyl → phenolic intermediates), after which H-transfer hydrogenation saturates the aromatic ring to give alkyl-substituted cyclohexanols. In parallel, the aryl propyl sidechain can shorten by H-transfer-hydrogenolysis, so the initially dominant formation of 4-(3-hydroxypropyl)cyclohexanol can diverge to the generation of ethyl phenol and 4-ethylcyclohexanol at longer times (main product when using fresh catalyst).[9,32,36,37,44,45] Note that the H-transfer saturation of syringyl and guaiacyl intermediates to the corresponding 2(,6)-(di)methoxy-4-alkyl-cyclohexanols is unlikely to take place in the presence of RANEY® Ni using 2-propanol as the H-donor.[29,38] (b) Time-resolved evolution of monomer yields during HT-RCF of post-consumer cardboard. Stacked bars show total monomer yield (GC-FID/MS) at 200 °C as a function of reaction time. Colours distinguish intermediate phenols (red scale) from cyclohexanol products (blue scale), further resolved by side-chain substituent at R (legend). (b) Shows that HT-RCF of cardboard at 200 °C begins producing phenolic monomers during heat-up, which peak within 1 h and then decline as they convert into alkyl phenols. With longer times, aromatic saturation dominates, yielding cyclohexanols, shifting from 4-(3-hydroxypropyl)cyclohexanol early to 4-ethylcyclohexanol after 3–4 h.

implies that RANEY® Ni remains active long enough to process the monomer pool, a behaviour not routinely observed for unprocessed biomass. These kinetic baselines set the stage for the subsequent recycling study, where changes in hydrogenation performance can be interpreted against this established sequence of intermediate formation and consumption.[9,32,36,37,44,45]

Fig. 6 shows that, in the recycling experiments, the ring-saturation function of RANEY® Ni undergoes rapid attenuation after the initial use. The product distribution shifts markedly from being cyclohexanols-rich in the 1st run to phenolic-rich from the 2nd run onwards. The near-constant total monomer yield indicates that lignin depolymerisation, ether cleavage, and lignin stabilisation pathways remain active across cycles. However, their products are no longer upgraded to cyclohexanols once the ring-saturation capacity declines.

Considering the GPC data (Fig. 7), all HT-RCF oils exhibit a relatively narrow, monomer-centred envelope with a maximum around 18–19 min, whereas the organosolv oil shows a broader distribution with a pronounced tail at shorter elution times (14–16 min), reflecting the polymeric nature of the isolated lignin. In the 1st run (fresh catalyst) the 280 nm absorbance is weak across the SI window, consistent with the extensive saturation of phenolic rings to cyclohexanol derivatives, which carry negligible absorbance at 280 nm. Upon recycling, the intensity at 280 nm increases markedly in the same elution time window, evidencing the accumulation of phenolic monomer products as the hydrogenation function diminishes. In the 2nd–5th runs, the product distribution remains essentially unchanged while the 280 nm intensity stabilises. This observation agrees well with our initial results in HT-RCF of poplar
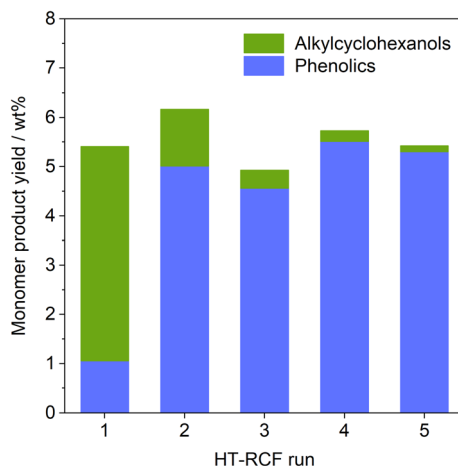
Fig. 6 Catalyst recycling in HT-RCF of post-consumer cardboard: evolution of monomer product yields. Stacked bars show GC-FID/MS monomer yields (wt%) over five consecutive HT-RCF runs with magnetically recovered RANEY® Ni in 2-propanol/H_2O (7:3, v/v) at 200 °C, 3 h, H_2-free. Run 1 is dominated by alkylcyclohexanols (4–4.5 wt%) with a small phenolic fraction (1 wt%), evidencing vigorous hydrogenation activity. Upon catalyst reuse (runs 2–5), the hydrogenated fraction drops sharply (≤1.2 → 0.1 wt%), while phenolic yields rise (5 wt%) and remain dominant. The total monomer yield remains broadly constant (≈5–6 wt%), indicating that solvolysis/HDO persists, whereas the ring saturation function of RANEY® Ni diminishes after the first cycle.
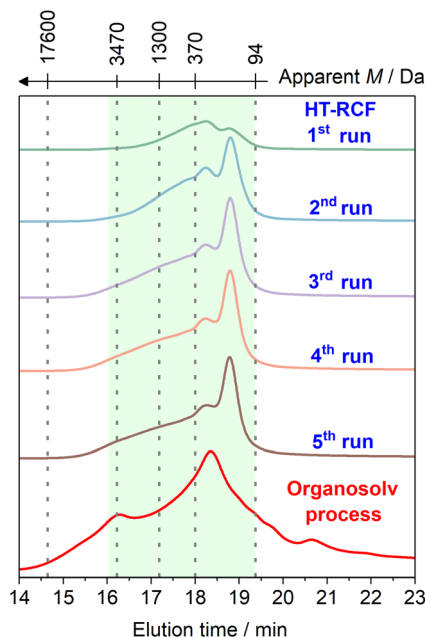
Fig. 7 GPC–UV analysis of HT-RCF lignin oils. Size-exclusion chromatograms (UV detection at 280 nm) of lignin oils from HT-RCF of post-consumer cardboard over five consecutive runs (RANEY® Ni; 2-propanol/H_2O, 7 : 3 v/v; 200 °C, 3 h) alongside an organosolv reference. For consistency, the green-shaded band marks the elution window used to calculate $SI_{320}(M)$ profiles. Mean ± s.d. values were derived from all data points within the indicated elution window and are reported for each sample in Fig. 9.

wood, showing that RANEY® Ni could be recycled up to 8 times with no perceived changes in both GPC separation profiles and the isolated yield of lignin oil.[7]

Fig. 8 presents the $SI_{320}(M)$ profiles for the lignin streams obtained for HT-RCF catalyst recycling experiments and organosolv lignin as the baseline comparison. The fresh catalyst (1st run) displays the highest SI_{320} across the monomer elution window, consistent with a product slate depleted in conjugated chromophores. Although the absolute UV absorbance at 280 nm is very weak in the 1st run (Fig. 7), the index captures the extensive chromophore depletion in the remnant lignin-derived fragments. Upon RANEY® Ni recycling (2nd–5th runs) the $SI_{320}(M)$ profiles remain converged toward the initial SI_{320} in the phenolic monomer products' window (18.0–19.0 min), confirming the data from Fig. 6, which indicate similar levels of phenolic products due to the marked decrease in ring saturation capacity. Conversely, a gradual reduction in the SI_{320} detected for lignin species eluting at times shorter than 18.5 min demonstrates that, although the phenolic monomer yields remain stable, the ageing of the catalyst causes a gradual reduction in the overall catalytic activity.

The organosolv oil exhibits the lowest SI_{320} baseline throughout, which is anticipated for a process that does not stabilise lignin, thereby not preventing the formation of chromophore centres. Combined with the monomer yields (Fig. 6)
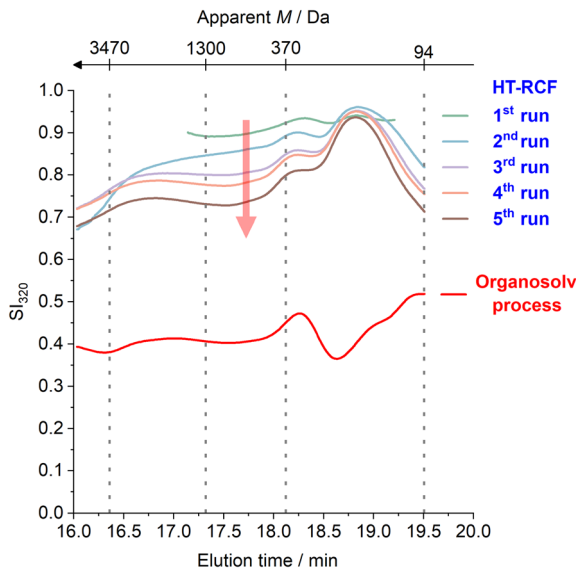
Fig. 8 $SI_{320}(M)$ profiles of HT–RCF lignin oils from post-consumer cardboard obtained over five consecutive HT–RCF runs with RANEY® Ni (2-propanol/H$_2$O, 7:3 v/v; 200 °C; 3 h; H$_2$-free), compared with the $SI_{320}(M)$ profile of organosolv lignin.

and the GPC–UV trends (Fig. 7), Fig. 8 indicates that SI_{320} is a sensitive, M-resolved marker of catalyst ageing in RCF. Mechanistically, the catalyst ageing appears to be selective. Surface modifications that inhibit ring saturation and demethoxy-lation (*e.g.*, site blocking/oxidation or compositional drift) occur more readily than those impairing hydrogenolysis and the selective HDO of carbonyl groups in lignin fragments.[36,37,44] Consequently, the release of phenolic monomers remains unaffected mainly while the catalyst maintains sufficient activity towards lignin stabilisation, preserving the overall monomer yield, as shown in Fig. 6.

Considering the mean values of SI_{320} in the selected M range presented in Fig. 7, the big picture of RANEY® Ni stability in the recycling experiments can be drawn (Fig. 9). Across the first five cycles, SI_{320} declines approximately linearly ($\approx 3.65 \times 10^{-2}$ per run). The linear regression of the mean values for SI_{320} generates a model ($r^2 = 0.95$) that enables a practical life estimate for the lignin stabilisation function of RANEY® Ni catalyst performance. Under the conditions of our experiments, the 15th run (*ca.* 45 h of HT-RCF operation), the mean value of SI_{320} is expected to match that of organosolv lignin, *i.e.*, the HT-RCF lignin would exhibit organosolv-like chromophore density. This demonstrates RANEY® Ni to be a very stable catalyst for the HT-RCF purpose, preventing lignin fragments from condensation.

While this is an extrapolation from five points and long-time behaviour may deviate from linearity, the result illustrates how SI_{320} serves as a direct, unified metric to compare catalyst/solvent effects in RCF experimental condition screening, an in-line diagnostic to schedule catalyst maintenance/regeneration, and may indeed help translate batch recycling experiment data into time-on-stream for continuous HT-RCF.
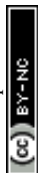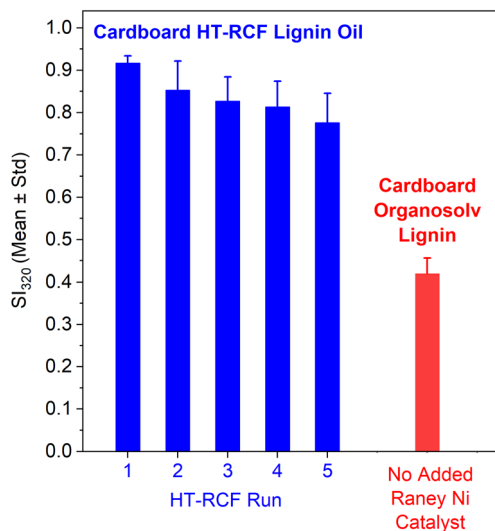
Fig. 9 Evolution of SI_{320} with catalyst recycle and linear deactivation model. A linear fit to SI_{320} *vs.* run count gives: $SI_{320} = (0.951 \pm 0.007) - (0.03652 \pm 0.00371) \times n$ ($r^2 = 0.95$), where "*n*" is the run number. Extrapolation to the mean value for organosolv lignin indicates convergence at approximately the 15th run, around 45 hours of HT-RCF operation.

Conclusions

We introduced SI_{320}, a simple, concentration-independent spectral index derived from UV–Vis. We demonstrated that—when coupled to GPC—it provides $SI_{320}(M)$ profiles for changes in lignin structure that accompany catalyst ageing in lignin-first processing. By including the absorbance at 320 nm into a ratio referenced to the aromatic band at 280 nm, SI_{320} selectively reports the build-up of degradation-related chromophores (*e.g.*, benzylic carbonyls, quinonoid species, extended π-systems) while remaining insensitive to sample loading within the Beer–Lambert regime.

In practical terms, high SI_{320} values correspond to oils depleted in conjugated chromophores—*i.e.*, strong lignin stabilisation—whereas declining SI_{320} values track the selective loss of lignin stabilisation function upon catalyst recycle. The cardboard case study demonstrates that SI_{320} detects ageing before bulk KPIs or total monomer yields diverge, and that its trend can be rendered quantitative (here, an approximately linear decrease across the first five cycles) to estimate useful hydrogenation life under batch conditions (*ca.* 15 runs, corresponding to 45 h of HT-RCF under our experimental conditions).

Beyond serving as a sensitive ageing marker, SI_{320} bridges analytics and operations for several reasons. First, the $SI_{320}(M)$ profiles reveal where in the product distribution chromophores accrue (monomer window *vs.* heavier fractions), enabling mechanism-aware mitigation (*e.g.*, solvent composition, hydrogen-donor strength, H_2 pressure, co-catalysts). Second, because SI_{320} determination is fast and non-destructive, it is well suited for in-line quality control. Acceptance windows for SI_{320} (and its variance within a defined M window) can be tied to desired oil attributes, whether for downstream monomer
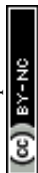
chemistry or for recovering stabilised oligomers. Third, SI_{320} integrates naturally with established pulp metrics (delignification, glucan/xylan retention) and product analytics (GC-FID/MS), providing a compact fingerprint that links catalyst state, lignin oil quality, and fibre preservation within one framework.

We emphasise that SI_{320} complements, rather than replaces, advanced structural methods such as HSQC NMR. It excels where small amounts of dispersed chromophores are otherwise hard to quantify, and it does so with minimal sample preparation. Limitations are clear and tractable—selection of M window; verification of Beer–Lambert linearity; and care in comparing datasets across instruments and eluents. With these caveats observed, SI_{320} offers a practical, transferable metric for monitoring and managing catalyst performance in lignin-first processes. Its use should facilitate more durable RCF operations, improve product consistency, and, ultimately, accelerate lignin valorisation by linking routine UV–Vis spectroscopy to actionable decisions on catalyst regeneration, process tuning, and feedstock selection.

Conflicts of interest

The authors declare no conflict of interest.

Data availability

All the data corresponding to this study have been included in the paper.

Acknowledgements

References

1 A. J. Ragauskas, G. T. Beckham, M. J. Biddy, R. Chandra, F. Chen, M. F. Davis, B. H. Davison, R. A. Dixon, P. Gilna, M. Keller, P. Langan, A. K. Naskar, J. N. Saddler, T. J. Tschaplinski, G. A. Tuskan and C. E. Wyman, *Science*, 2014, **344**, 1246843, DOI: **10.1126/science.1246843**.

2 R. Rinaldi, R. Jastrzebski, M. T. Clough, J. Ralph, M. Kennema, P. C. A. Bruijnincx and B. M. Weckhuysen, *Angew. Chem., Int. Ed.*, 2016, **55**, 8164–8215.

3 Z. Sun, B. Fridrich, A. De Santi, S. Elangovan and K. Barta, *Chem. Rev.*, 2018, **118**, 614–678.

4 W. Schutyser, T. Renders, S. Van den Bosch, S.-F. Koelewijn, G. T. Beckham and B. F. Sels, *Chem. Soc. Rev.*, 2018, **47**, 852–908.

5 M. M. Abu-Omar, K. Barta, G. T. Beckham, J. S. Luterbacher, J. Ralph, R. Rinaldi, Y. Román-Leshkov, J. S. M. Samec, B. F. Sels and F. Wang, *Energy Environ. Sci.*, 2021, **14**, 262–292.

6 R. Rinaldi, in *Lignin Valorization: Emerging Approaches*, RSC Energy and Environment Series, ed. G. T. Beckham, Royal Society of Chemistry, 2018, ch. 5, pp. 108–127.
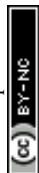
7 P. Ferrini and R. Rinaldi, *Angew. Chem., Int. Ed.*, 2014, **53**, 8634–8639.

8 M. T. Amiri, S. Bertella, Y. M. Questell-Santiago and J. S. Luterbacher, *Chem. Sci.*, 2019, **10**, 8135–8142.

9 R. Rinken, D. Posthuma and R. Rinaldi, *ChemSusChem*, 2023, **16**, e202201875, DOI: **10.1002/cssc.202201875**.

10 R. Rinaldi, *Angew. Chem., Int. Ed.*, 2014, **53**, 8559–8560.

11 Y. M. Questell-Santiago, M. V. Galkin, K. Barta and J. S. Luterbacher, *Nat. Rev. Chem.*, 2020, **4**, 311–330.

12 E. Cooreman, T. Vangeel, K. Van Aelst, J. Van Aelst, J. Lauwaert, J. W. Thybaut, S. Van Den Bosch and B. F. Sels, *Ind. Eng. Chem. Res.*, 2020, **59**, 17035–17045.

13 J. Ralph, C. Lapierre and W. Boerjan, *Curr. Opin. Biotechnol.*, 2019, **56**, 240–249.

14 M. Sette, H. Lange and C. Crestini, *Comput. Struct. Biotechnol. J.*, 2013, **6**, e201303016.

15 J. L. Wen, S. L. Sun, B. L. Xue and R. C. Sun, *Materials*, 2013, **6**, 359–391.

16 R. M. Happs, B. Addison, C. Doeppke, B. S. Donohoe, M. F. Davis and A. E. Harman-Ware, *Biotechnol. Biofuels*, 2021, **14**, 58, DOI: **10.1186/s13068-021-01897-y**.

17 F. Bugli, A. Baldelli, S. Thomas, M. Sgarzi, M. Gigli, C. Crestini, F. Cavani and T. Tabanelli, *ACS Sustain. Chem. Eng.*, 2024, **12**, 16638–16651.

18 M. Sette, R. Wechselberger and C. Crestini, *Chem.–Eur. J.*, 2011, **17**, 9529–9535.

19 A. Granata and D. S. Argyropoulos, *J. Agric. Food Chem.*, 1995, **43**, 1538–1544.

20 J. K. Kenny, J. W. Medlin and G. T. Beckham, *ACS Sustain. Chem. Eng.*, 2023, **11**, 5644–5655.

21 H. Zhang, S. Fu and Y. Chen, *Int. J. Biol. Macromol.*, 2020, **147**, 607–615.

22 S. Y. Lin, in *Methods in Lignin Chemistry*, ed. S. Y. Lin and C. W. Dence, Springer, Berlin, Heidelberg, 1992, pp. 217–232.

23 A. Sluiter, B. Hames, R. Ruiz, C. Scarlata, J. Sluiter, D. Templeton and D. Crocker, *Determination of Structural Carbohydrates and Lignin in Biomass*, Laboratory Analytical Procedure (LAP), National Renewable Energy Laboratory, 2008.

24 A. Sluiter, B. Hames, R. Ruiz, C. Scarlata, J. Sluiter and D. Templeton, *Determination of Ash in Biomass*, Laboratory Analytical Procedure (LAP), National Renewable Energy Laboratory, 2008.

25 C. S. Kim, O. W. Kwon, S. Y. Kim and K. R. Lee, *J. Nat. Prod.*, 2013, **76**, 2131–2135.

26 B. Wu and J. Wang, *Chem. Biodiversity*, 2011, **8**, 1735–1747.

27 Y.-H. Wang, Q.-Y. Sun, F.-M. Yang, C.-L. Long, F.-W. Zhao, G.-H. Tang, H.-M. Niu, H. Wang, Q.-Q. Huang, J.-J. Xu and L.-J. Ma, *Helv. Chim. Acta*, 2010, **93**, 2467–2477.

28 S. Ralph and J. Ralph, NMR Database of Lignin and Cell Wall Model Compounds, 2009, available at: **https://www.glbrc.org/databases_and_software/nmrdatabase/**, accessed August 2025.

29 X. Wang and R. Rinaldi, *Energy Environ. Sci.*, 2012, **5**, 8244–8260.

30 E. M. Anderson, M. L. Stone, R. Katahira, M. Reed, W. Muchero, K. J. Ramirez, G. T. Beckham and Y. Román-Leshkov, *Nat. Commun.*, 2019, **10**, 2033.

31 Z. Liu, H. Li, X. Gao, X. Guo, S. Wang, Y. Fang and G. Song, *Nat. Commun.*, 2022, **13**, 4716.

32 X. Wang and R. Rinaldi, *ChemSusChem*, 2012, **5**, 1455–1466.

33 A. Lähdetie, T. Liitiä, T. Tamminen and A.-S. Jääskeläinen, *BioResources*, 2009, **4**, 1600–1619.

34 J. Schmidt, in *Lignin and Lignans: Advances in Chemistry*, ed. C. Heitner, D. Dimmel and J. Schmidt, CRC Press, Boca Raton, 2010, ch. 3, pp. 49–102.

35 J. Hynynen, A. Riddell, A. Achour, Z. Takacs, M. Wallin, J. Parkås and D. Bernin, *Green Chem.*, 2021, **23**, 8251–8259.

36 M. Kennema, I. B. D. de Castro, F. Meemken and R. Rinaldi, *ACS Catal.*, 2017, **7**, 2437–2445.

37 G. Calvaruso, J. A. Burak, M. T. Clough, M. Kennema, F. Meemken and R. Rinaldi, *ChemCatChem*, 2017, **9**, 2627–2632.

38 X. Wang and R. Rinaldi, *Angew. Chem., Int. Ed.*, 2013, **52**, 11499–11503.

39 F. Lu, C. Wang, M. Chen, F. Yue and J. Ralph, *Green Chem.*, 2021, **23**, 5106–5112.

40 Confederation of Paper Industries, *2021–22 Annual Review*, 2023.

41 J. Y. Keränen and E. Retulainen, *BioResources*, 2016, **11**, 10404–10418.

42 I. Graça, R. T. Woodward, M. Kennema and R. Rinaldi, *ACS Sustain. Chem. Eng.*, 2018, **6**, 13408–13419.

43 C. Chesi, I. B. D. de Castro, M. T. Clough, P. Ferrini and R. Rinaldi, *ChemCatChem*, 2016, **8**, 2079–2088.

44 I. B. D. de Castro, I. Graça, L. Rodríguez-García, M. Kennema, R. Rinaldi and F. Meemken, *Catal. Sci. Technol.*, 2018, **8**, 3107–3114.

45 P. Ferrini, C. Chesi, N. Parkin and R. Rinaldi, *Faraday Discuss.*, 2017, **202**, 403–413.

46 L. Ramazanova, L. Reimund, D. Lebedeva, S. Muangmeesri, A. Jaworski and J. S. M. Samec, *ACS Sustain. Chem. Eng.*, 2024, **12**, 13409–13414.

47 I. Kumaniaev, E. Subbotina, J. Sävmarker, M. Larhed, M. V. Galkin and J. S. M. Samec, *Green Chem.*, 2017, **19**, 5767–5771.

48 E. M. Anderson, M. L. Stone, R. Katahira, M. Reed, G. T. Beckham and Y. Román-Leshkov, *Joule*, 2017, **1**, 613–622.

49 J. H. Jang, D. G. Brandner, R. J. Dreiling, A. J. Ringsby, J. R. Bussard, L. M. Stanley, R. M. Happs, A. S. Kovvali, J. I. Cutler, T. Renders, J. R. Bielenberg, Y. Román-Leshkov and G. T. Beckham, *Joule*, 2022, **6**, 1859–1875.